

# A Binary-Based Reassessment of the Age and Stellar Properties of NGC 7789 Using Twelve Binary Components

Kadri Yakut,<sup>1,2</sup>\* Belinda Kalomeni<sup>1</sup> and Saul Rappaport<sup>3</sup>

<sup>1</sup>Department of Astronomy and Space Sciences, Faculty of Science, Ege University, 35100, Izmir, Türkiye

<sup>2</sup>Institute of Astronomy, The Observatories, Madingley Road, Cambridge CB3 0HA, UK

<sup>3</sup>Department of Physics, Kavli Institute for Astrophysics and Space Research, M.I.T., Cambridge, USA

arXiv:2601.16265v1 [astro-ph.SR] 22 Jan 2026

Accepted XXX. Received YYY; in original form ZZZ

## ABSTRACT

We present a binary-based reassessment of the age of the intermediate-age open cluster NGC 7789, together with well-constrained stellar parameters for twelve components in six SB2 systems, including two eclipsing binaries. Our analysis employs a unified modelling framework that combines radial-velocity orbits, TESS light curves, and blue-to-IR spectral energy distributions (SEDs), providing a robust alternative to traditional isochrone-based age determinations. By adopting common cluster-wide parameters (age, distance, and line-of-sight extinction) when solving for the stellar parameters of the binary components, we obtain a coherent set of masses, radii, effective temperatures, and luminosities for all twelve stars. The combined SED, eclipsing-binary, and radial-velocity analysis yields a well-constrained cluster age of  $1.26 \pm 0.09$  Gyr and an extinction of  $A_V = 0.90 \pm 0.05$  mag, while remaining consistent with the *Gaia* DR3 distance of  $d \simeq 2.06$  kpc used as an external prior. An independent *Gaia* DR3 astrometric analysis gives a distance of  $2082 \pm 142$  pc and confirms the membership of all six systems. The twelve binary components occupy the turnoff and subgiant regions of the cluster, enabling stringent evolutionary tests: in the radius–mass, radius–temperature, and temperature–mass diagrams, they show excellent agreement with modern stellar evolution models for the derived cluster parameters. NGC 7789 has long been affected by age discrepancies arising from MSTO broadening, rotation, and differential reddening, with literature estimates spanning 1.1 to 1.6 Gyr. Our binary-anchored analysis significantly narrows this range and demonstrates that a self-consistent set of parameters emerges when dynamical SB2 information, eclipsing-binary geometry, and SED constraints are jointly analyzed. NGC 7789 thus serves as a valuable benchmark for multi-observable, binary-based age determinations in open cluster studies.

**Key words:** Binary stars — Fundamental parameters of stars — (Galaxy:) open clusters and associations: individual (NGC 7789) — (Galaxy:) open clusters and associations: general — proper motions

## 1 INTRODUCTION

Open clusters serve as fundamental laboratories for testing stellar evolution theory, calibrating age–activity and age–rotation relations, and tracing the chemical and dynamical history of the Galactic disk. Their ages are therefore of central importance, yet age determinations remain sensitive to the adopted methodology. Traditionally, the ages of open clusters have been inferred through (i) isochrone fitting to colour–magnitude diagrams, (ii) asteroseismic constraints, (iii) white-dwarf cooling sequences, (iv) gyrochronology, and (v) eclipsing-binary (EB) based age determinations, which exploit precisely measured stellar masses and radii. Each of these has its own advantages and systematic limitations. In two recent studies (Yakut et al. 2025a,b), we introduced a complementary, physically grounded approach in which the ages of clusters are derived by jointly modelling the spectral energy distributions (SEDs), radial velocities (RVs), and (when available) light curves (LCs) of multiple double-lined binary systems. Because this method relies on stellar masses, radii, and tem-

peratures that are tightly constrained by binary dynamics and multi-observable modelling—rather than on CMD morphology alone—it provides an independent and sensitive probe of cluster ages. We first applied this technique to the old open cluster NGC 188 (see also the case of the very old open cluster NGC 6791; Yakut et al. 2015), obtaining an age of  $6.41 \pm 0.33$  Gyr, and subsequently to the intermediate-age cluster NGC 2506, deriving  $1.94 \pm 0.03$  Gyr. In the present work, we extend the same methodology to the younger cluster NGC 7789.

NGC 7789 ( $\alpha_{J2000} = 23^{\text{h}}57^{\text{m}}19^{\text{s}}$ ,  $\delta_{J2000} = +56^{\circ}43'28''$ ) is a rich, well-studied, intermediate-age open cluster located in the constellation Cassiopeia (Anthony-Twarog et al. 2025; Friel et al. 2002; Nagarajan et al. 2023). With Galactic coordinates  $(l, b) \approx (115.5^{\circ}, -5.4^{\circ})$  (Ferreira et al. 2025), the cluster lies in the direction of the Galactic anticentre and serves as an important benchmark system for tracing stellar evolution and Galactic disk chemo-dynamics. NGC 7789 hosts a dense stellar population, including a well-developed main-sequence turnoff (MSTO), a prominent red giant branch, and an unusually large population of blue straggler stars (BSS) (Anthony-Twarog et al. 2025; Friel et al. 2002). Estimates

\*E-mail: kadri.yakut@ege.edu.tr (KY)

based on deep Gaia photometry suggest that the cluster may contain as many as  $\sim 3000$  members down to  $G \approx 21$  mag (Gao 2018), making it one of the richer intermediate-age clusters in the solar neighbourhood.

Historically, the cluster was first studied photometrically by Burbridge & Sandage (1958) using *UBV* photometry for nearly 700 stars, yielding an early reddening estimate of  $E(B-V) = 0.24$ . Modern combined photometric and Gaia-based analyses have revised this value upward: Anthony-Twarog et al. (2025) reported  $E(B-V) = 0.30 \pm 0.02$ , and Ferreira et al. (2025) derived  $E(B-V) = 0.328 \pm 0.008$  from Gaia DR3 data. NGC 7789 is known to be affected by substantial interstellar reddening owing to its relatively low Galactic latitude, which has long complicated its photometric interpretation.

Chemical abundance studies indicate that NGC 7789 has an overall near-solar iron abundance. Early photometric metallicity estimates suggested subsolar values, such as  $[\text{Fe}/\text{H}] = -0.26 \pm 0.10$  (Friel et al. 2002), whereas modern high-resolution spectroscopic analyses consistently converge toward solar composition, including  $[\text{Fe}/\text{H}] = -0.04 \pm 0.05$  (Tautvaišienė et al. 2005a) and  $[\text{Fe}/\text{H}] = +0.02 \pm 0.04$  (Jacobson et al. 2011). At the same time, detailed chemical studies reveal that the cluster is not chemically simple, showing significant enhancements in neutron-capture elements—particularly barium—with  $[\text{Ba}/\text{Fe}] \approx +0.47$  to  $+0.48$  (Overbeek et al. 2015; Pancino et al. 2010), along with mild  $\alpha$ -element enrichment and evolutionary C–N–O abundance patterns associated with dredge-up and extra mixing processes (e.g., Overbeek et al. 2015; Nagarajan et al. 2023).

Estimates of the cluster’s age vary across the literature. Traditional photometric analyses based on colour–magnitude diagram fitting have typically yielded ages in the range 1.4–1.6 Gyr (e.g. Gim et al. 1998; Ferreira et al. 2025). Using *Gaia* DR2 astrometry and homogeneous isochrone fitting, Cantat-Gaudin et al. (2020) derived an age of  $\sim 1.2$  Gyr for NGC 7789, highlighting the sensitivity of the inferred age to the adopted methodology and treatment of extinction. Evidence has also been presented for an extended main–sequence turnoff (eMSTO): de Juan Ovelar et al. (2020) interpreted the observed MSTO width as corresponding to an age spread of  $\sim 390$  Myr, suggesting a representative age of  $1070 \pm 390$  Myr, although the interpretation remains debated and may be linked to stellar rotation, overshooting, or differential reddening (Anthony-Twarog et al. 2025). Overall, the dispersion in published age estimates primarily reflects the combined effects of differential reddening, high binary fraction, and rotation–driven broadening of the MSTO. For clarity, a consolidated summary of previously published age, distance, metallicity, and reddening estimates for NGC 7789 is provided in Table 1.

Radial-velocity surveys have played a central role in establishing cluster membership and identifying binary systems. The WIYN Open Cluster Study (WOCS) survey identified 624 likely members and derived orbits for 81 spectroscopic binaries with orbital periods ranging from 1.45 to 4200 days (Nine et al. 2020). From these surveys we selected six SB2 systems with secure Gaia DR3 membership, well-determined RV curves, and reliable broad-band SED coverage. The systemic radial velocity of the cluster lies between  $-54$  and  $-58$   $\text{km s}^{-1}$ , with a consensus value of approximately  $-54.5 \text{ km s}^{-1}$ .

Binary evolution is known to play a fundamental role in shaping the observed properties of star clusters, affecting both their colour–magnitude morphologies and the interpretation of cluster ages. Theoretical and population–synthesis studies have long shown that mass transfer, angular momentum loss, and mergers in binary systems can substantially alter stellar evolutionary paths, producing rejuvenated stars and blue straggler populations that deviate from single-star

isochrones (e.g., Hurley et al. 2001; Yakut et al. 2009). Observationally, blue straggler stars are therefore widely regarded as indirect tracers of past and ongoing binary interaction in clusters (e.g., Ferraro et al. 2009; Perets & Fabrycky 2009). In NGC 7789, ultraviolet observations have revealed hot companions and extremely low–mass white dwarfs in a significant fraction of blue stragglers, strongly supporting mass–transfer formation channels (Vaidya et al. 2022, 2024).

A consolidated overview of the literature values for age, metallicity, reddening, and distance is provided in Table 1, which summarizes results from both classical and modern investigations.

Modern Gaia-based analyses provide refined estimates of the distance and reddening of the cluster. Gaia-based studies place the cluster at a distance of  $\sim 2.1$  kpc (e.g. Cantat-Gaudin et al. 2018; Nine et al. 2020), consistent with more recent DR3 analyses. Similarly, reddening estimates put the cluster in the range 0.27–0.33 mag, consistent with recent high-quality photometry and spectroscopy.

In two recent studies of NGC 188 and NGC 2506, we demonstrated that combining spectroscopic orbital solutions with broad-band spectral energy distributions of multiple binary systems provides a powerful and physically grounded alternative to traditional isochrone fitting (Yakut et al. 2025a,b). This joint RV+LC+SED methodology yields self-consistent cluster ages, distances, and extinction values by using directly measured stellar masses and radii rather than inferring them from photometry alone. In the present study of NGC 7789, by anchoring the cluster parameters to six binaries comprising twelve well-characterised stellar components, we obtain one of the most precise and dynamically validated determinations of the cluster age to date.

In the present study, we apply the same methodology to NGC 7789 using six double-lined spectroscopic binaries, including two eclipsing systems for which joint light-curve and radial-velocity solutions can be obtained. Section 2 describes the observational material used in this work. Section 3 presents the radial-velocity and light-curve modelling. Section 4 introduces the SED analysis and joint fitting framework. Section 5 summarizes the Gaia-based astrometric validation. Section 6 discusses the combined results and their implications for the age, distance, reddening, and chemical composition of NGC 7789.

## 2 OBSERVATIONS

The observational data used in this study consist of three complementary components: (1) TESS photometry, (2) ground-based spectroscopic radial–velocity (RV) measurements, and (3) broad-band spectral energy distributions assembled from archival surveys. These datasets provide independent and mutually constraining diagnostics on the physical properties of the six binary systems analysed in this work. Basic astrometric and photometric information for all six double-lined spectroscopic binaries considered in this study is summarised in Table 2.

### 2.1 Radial–Velocity Measurements

High–resolution spectroscopy for all six binary systems was obtained by Nine et al. (2020), who provided double-lined RV measurements for both the primary and secondary components. These data form the basis of our orbital solutions (Sect. 3). We adopted the heliocentric Julian dates (HJDs), RVs, and published measurement weights (CH values), but performed our fits using both weighted and unweighted approaches to ensure robustness. The phase–folded RV curves and

**Table 1.** Summary of derived parameters for the NGC 7789 open cluster from past and recent investigations.

Age Gyr	Distance kpc	[Fe/H] dex	$E(B - V)$ mag	Reference
1.1	1.86		0.35	<a href="#">Mazzei &amp; Pigatto (1988)</a>
1.2	$2.45 \pm 0.15$		$0.33 \pm 0.03$	<a href="#">Martinez Roger et al. (1994)</a>
		$-0.04 \pm 0.05$		<a href="#">Tautvaišienė et al. (2005b)</a>
1.2	$2.08 \pm 0.01$	+0.023		<a href="#">Cantat-Gaudin et al. (2018)</a>
1.4	1.80		0.28	<a href="#">Gao (2018)</a>
$1.61 \pm 0.05$	$1.91 \pm 0.03$	+0.026	$0.31 \pm 0.02$	<a href="#">Dias et al. (2021)</a>
1.2	1.8	+0.023	0.27	<a href="#">Nine et al. (2020)</a>
1.07			$-0.013 \pm 0.023$	<a href="#">de Juan Ovelar et al. (2020)</a>
$1.42 \pm 0.12$	$1.92 \pm 0.08$		0.28	<a href="#">Spina et al. (2021)</a>
		$-0.02 \pm 0.05$		<a href="#">Vaidya et al. (2022)</a>
		$0.00 \pm 0.07$		<a href="#">Nagarajan et al. (2023)</a>
$1.60 \pm 0.10$	1.90	$0.04 \pm 0.05$		<a href="#">Carbajo-Hijarrubia et al. (2024)</a>
		$-0.01 \pm 0.04$		<a href="#">Balan et al. (2024)</a>
$1.51 \pm 0.20$	$1.91 \pm 0.03$	$+0.05 \pm 0.07$	$0.328 \pm 0.008$	<a href="#">Nine et al. (2024)</a>
				<a href="#">Ferreira et al. (2025)</a>
$1.34 \pm 0.18$	$1.96 \pm 0.21$	$+0.01 \pm 0.03$	$0.31 \pm 0.03$	Mean $\pm$ std. dev.
$1.26 \pm 0.09$	...	$\gtrsim +0.1$	$0.29 \pm 0.02$	This study

the best-fitting orbital models are displayed in Figure 1. The derived orbital parameters for the six systems are summarised in Table 3.

## 2.2 TESS Photometry

NGC 7789 was observed by the *Transiting Exoplanet Survey Satellite* (TESS) during Sectors 17 and 24. We extracted light curves for all six target systems using the publicly available TASOC and SPOC pipelines, and subsequently performed detrending and outlier removal following the procedures described in our earlier cluster studies. Among the six systems, only two — WOCS 17028 and WOCS 14014 — exhibit detectable eclipses in the TESS photometry. For these two binaries, we carried out a full eclipsing-binary analysis (Sect. 3), while for the remaining four systems the TESS fluxes were used solely for variability checks and contamination assessment. The phase-folded TESS light curves for the two eclipsing systems are shown in Figure 2, where the insets highlight the eclipse minima.

## 2.3 Spectral Energy Distributions

We constructed broadband SEDs for all six binaries using archival photometry compiled through the VizieR database (Ochsenbein et al. 2000). The dataset spans the ultraviolet to the infrared, drawing on measurements from GALEX (Bianchi et al. 2017), APASS (Henden et al. 2016), Pan-STARRS (Chambers et al. 2016), 2MASS (Skrutskie et al. 2006), and WISE (Cutri et al. 2013). For each system, the photometry was assembled using *Gaia* DR3 source identifiers to ensure a consistent and unambiguous association of flux measurements across all wavelength bands. The final SEDs, shown in Figure 3, exhibit smooth flux distributions with no significant discontinuities between adjacent passbands, except perhaps at the Balmer discontinuity near 3645 Å. These SEDs form one of the three pillars of our joint SED+EB+RV modelling approach (Sect. 4), providing strong constraints on stellar luminosities, radii, and effective temperatures.

Together, the TESS photometry, high-precision RV orbits, and broadband SEDs constitute a complete and complementary observational framework. This multi-observable dataset enables the si-

multaneous determination of the stellar and orbital properties of the six binaries, while also providing the foundation for the global cluster-parameter inference presented in the subsequent sections.

## 3 LIGHT AND RADIAL VELOCITY CURVE MODELING

The spectroscopic orbital solutions for all six SB2 systems were derived from the complete set of radial-velocity (RV) measurements published by Nine et al. (2020). Since the original RV files list a third-column quantity (“CH”) rather than formal measurement uncertainties, we adopted two complementary strategies. Our primary analysis employed strictly unweighted RV fits in order to avoid propagating unknown or non-standard error estimates into the orbital solution. A secondary set of tests was performed in which the radial-velocity uncertainties were uniformly increased to assess the sensitivity of the fitted semi-amplitudes to reasonable changes in the assumed error scale. For each binary, an initial least-squares solution was followed by a full Markov Chain Monte Carlo (MCMC) exploration of the posterior distributions. The resulting orbital elements, including  $(K_1, K_2)$ , systemic velocity, and eccentricity when significant, are listed in Table 3.

Among the six systems, only WOCS 14014 and WOCS 17028 exhibit eclipses in the available TESS photometry. For these two sources, we performed a joint LC+RV solution using the MCMC-refined RV orbits as dynamical anchors. This combined modelling yields purely geometric constraints on the absolute masses and radii, independent of stellar evolutionary calculations, and provides a robust foundation for the subsequent SED-based inference. For the remaining four systems, only RV constraints were used, and their masses remain tied to the SED+evolution-track solution discussed in Sect. 4. The modelled lightcurves for WOCS 14014 and 17028 are compared to the TESS data in Fig. 2. We also tested solutions in which a third-light contribution ( $\ell_3$ ) was treated as a free parameter. In both systems, the fits converged to negligible or non-physical values ( $\ell_3 \leq 0$  for WOCS 17028 and  $\ell_3 \simeq 0$  for WOCS 14014), indicating that no detectable photometric third-light contribution is supported by the data.

**Table 2.** Astrometric and photometric properties of the six double-lined binary systems analyzed in this study, including Gaia DR3 and TESS IDs, proper motions, parallaxes, and Gaia colours.

	WOCS 17028 A	WOCS 14014 B	WOCS 8016 C	WOCS 14007 D	WOCS 17008 E	WOCS 31015 F
TIC ID	417031808	65558198	416814228	416814233	416814240	65558397
Gaia DR3 ID	1995020800153469568	1995061104128742272	1995066086290711424	1995010835829510144	1995010938908725376	1995013000492937984
Alias	NGC 7789 XZD 19	V874 Cas	NGC 7789 521	UCAC4 734-105175	J235747.61+564142.3	
$\alpha$ (°)	359.683	359.134	359.300	359.419	359.448	359.132
$\delta$ (°)	+56.851	+56.738	+56.853	+56.689	+56.695	+56.675
$\mu_\alpha$ (mas yr <sup>-1</sup> )	-0.815	-0.672	-0.945	-0.721	-0.699	-0.698
$\mu_\delta$ (mas yr <sup>-1</sup> )	-2.016	-1.916	-1.827	-2.009	-1.898	-1.786
$\varpi$ (mas)	0.4697	0.4795	0.4777	0.4495	0.4728	0.4840
$G$ (mag)	13.769	13.828	13.320	13.719	13.427	14.572
$G_{\text{BP}} - G_{\text{RP}}$ (mag)	0.925	0.905	0.982	0.854	0.955	0.931

In summary, the radial-velocity data provide the primary constraints on the orbital semi-amplitudes ( $K_1, K_2$ ) and mass ratios for all six systems, thereby defining the dynamical framework of each binary. The RV data plus the eclipses in two of the binaries lead directly to the determination of the masses and radii for four of the stars. For the other eight stars, the RV data primarily fix the mass ratios in each of these four binaries, and the SED analysis (see next section) is able to utilize this information to determine the masses for all twelve stars.

#### 4 JOINT SED FITTING FOR THE SIX BINARY SEDS

Before describing the individual SED fits, we briefly summarise the structure of the joint modelling; see also [Yakut et al. \(2025a,b\)](#) for further details. The analysis simultaneously solves for the parameters of all twelve stars together with a common set of cluster properties. The free parameters are: the masses of the twelve stars, and a global cluster age, distance (if the prior is opened up), extinction, and metallicity (usually left fixed), as well as the orbital inclinations of the four binaries without eclipses. This makes a total of between 18 and 20 free parameters to be determined. We utilise a Markov Chain Monte Carlo (MCMC) code to find the best fit to these parameters and their uncertainties.

The observational constraints comprise the following items: 12 RV semi-amplitudes ( $K_1$  and  $K_2$  for each of the six binaries), their orbital periods and eccentricities (taken to have negligible uncertainties), the orbital inclination angles for two of the six binaries, and approximately 150 broadband SED flux measurements spanning the blue to the mid-infrared.

The SED fitting code also utilizes stellar evolution constraints provided by MIST evolution tracks ([Choi et al. 2016; Dotter 2016; Paxton et al. 2011, 2015, 2019](#)) which link stellar mass, age, and metallicity to the stellar radii and effective temperatures. The synthetic spectral energy distributions are generated using the [Castelli & Kurucz \(2003\)](#) atmosphere models. In the present analysis, we adopted atmosphere grids computed at a fixed  $\log g = 4.0$  for all components. This choice is well justified, as the inferred surface gravities of our 12 stars stars have a mean  $\log g$  of 3.99 and an rms deviation from this value of 0.21 dex, implying a rather negligible impact on the derived SED-based parameters.

For each system, we compiled broadband photometry from the blue end of the spectrum to the mid-infrared (typically  $0.35 \mu\text{m} \lesssim \lambda \lesssim 12 \mu\text{m}$ ) using the VizieR SED interface ([Ochsenbein et al. 2000](#)). The data set includes fluxes from large-scale surveys such as GALEX ([Bianchi et al. 2017](#)), Pan-STARRS ([Chambers et al. 2016](#)), SDSS ([Gunn et al. 1998](#)), 2MASS ([Skrutskie et al. 2006](#)), WISE

([Cutri et al. 2013](#)), and *Gaia* ([Gaia Collaboration et al. 2023](#)), supplemented where available by additional published optical photometry from the literature. All measurements were retrieved from VizieR in a homogeneous absolute flux scale, with standard zero-point calibrations already applied. The photometry was then de-reddened using the current MCMC trial value of the cluster extinction. Because the photometry was taken non-simultaneously, and is subject to additional systematic effects (e.g. crowding, variability, and filter-transformation uncertainties), we imposed a minimum relative error floor of 5 per cent on all flux points, and adopted larger uncertainties for the most problematic bands (in particular the bluest point at  $0.35 \mu\text{m}$  and the longest-wavelength WISE measurements). We adopted a minimum uncertainty floor of 5 per cent because the formal catalogue uncertainties are typically at the sub-percent level and therefore do not capture the true level of systematic effects affecting multi-survey SEDs. Since the quoted catalogue uncertainties are much smaller than 5 per cent, it makes no practical difference whether they are added in quadrature or replaced by the adopted floor. Aside from the eclipse phases in the two eclipsing systems, no evidence is found for intrinsic broadband variability at a level that would require a larger error floor than the adopted 5 per cent.

The line-of-sight extinction  $A_V$  is treated as a single cluster-wide free parameter and is determined entirely from the joint SED fitting, rather than from the astrometric analysis. The adopted prior range on  $A_V$  (0.74–0.98) is motivated by previous photometric studies of NGC 7789 and serves only as a weak, physically informed constraint. As a robustness check, we repeated the SED analysis with a substantially widened range on the  $A_V$  prior (0.38–1.5). In this case, the posterior distribution shifts only slightly toward higher extinction values, while the inferred cluster age and stellar parameters remain unchanged within the quoted uncertainties. Given that unrealistically large extinctions are excluded by the literature, we therefore retain the adopted prior range in our final solution.

Photometric measurements at  $\lambda \simeq 0.23 \mu\text{m}$  are available for four of the six binaries analysed in this study; these points were excluded from the SED fitting for the following reason. At such short wavelengths, the interstellar extinction corrections along the line of sight to NGC 7789 reach nearly an order of magnitude, rendering the de-reddened fluxes highly sensitive to uncertainties in the adopted extinction law (e.g. [Cardelli et al. 1989](#)). As a result, the propagated flux uncertainties exceed the level of precision required for the present analysis and would otherwise dominate the  $\chi^2$  minimisation without providing commensurate physical constraints.

The fit to the SEDs proceeds roughly as follows. At each link of the MCMC chain, the 12 stellar masses are chosen, as well the age, distance, and extinction to the cluster. The MIST evolution tracks are then used to evaluate the corresponding stellar radii and  $T_{\text{eff}}$ .

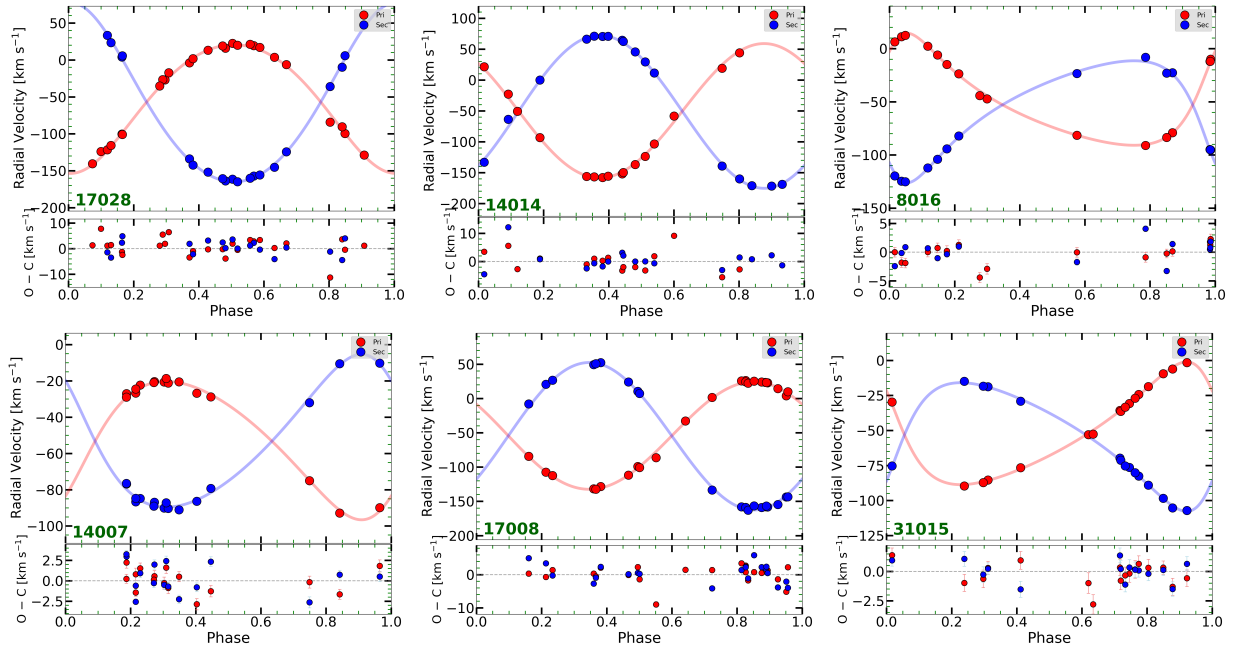


**Figure 1.** Observed (circles) and modelled (lines) radial velocities for the six selected binary systems in NGC 7789. Residuals (O-C) are shown below each panel. Red color denote the primary component, blue for the secondary.

**Table 3.** Orbital parameters of the six double-lined spectroscopic binary systems analyzed in this study. For each system, the following parameters are listed:  $K_1$  and  $K_2$  are the radial velocity semi-amplitudes of the primary and secondary components,  $P$  is the orbital period,  $e$  is the orbital eccentricity,  $\omega$  is the argument of periastron,  $T_0$  is the time of periastron passage, and  $\gamma$  is the systemic velocity

ID	$T_0$ (HJD - 2400000)	$P_{\text{orb}}$ (days)	$e$	$\omega$ (deg)	$V_\gamma$ (km s $^{-1}$ )	$K_1$ (km s $^{-1}$ )	$K_2$ (km s $^{-1}$ )
17028	$54711.7634 \pm 0.0107$	$3.55387 \pm 0.00001$	$0.115 \pm 0.004$	$173 \pm 1$	$-56.28 \pm 0.16$	$87.41 \pm 0.37$	$121.41 \pm 0.55$
14014	$55371.3462 \pm 0.0645$	$2.36602 \pm 0.00000$	$0.013 \pm 0.002$	$57 \pm 10$	$-50.11 \pm 0.20$	$109.20 \pm 0.42$	$123.86 \pm 0.31$
8016	$55313.3398 \pm 0.0428$	$30.97954 \pm 0.00086$	$0.409 \pm 0.005$	$312 \pm 1$	$-52.96 \pm 0.22$	$52.67 \pm 0.36$	$57.22 \pm 0.36$
14007	$54571.7490 \pm 0.1365$	$23.16631 \pm 0.00120$	$0.224 \pm 0.016$	$228 \pm 2$	$-53.13 \pm 0.22$	$38.64 \pm 0.70$	$42.40 \pm 0.75$
17008	$55011.4102 \pm 0.0746$	$2.76074 \pm 0.00000$	$0.009 \pm 0.001$	$43 \pm 10$	$-54.18 \pm 0.15$	$78.72 \pm 0.25$	$107.38 \pm 0.26$
31015	$55558.2274 \pm 0.1401$	$34.41091 \pm 0.00553$	$0.356 \pm 0.010$	$58 \pm 2$	$-53.26 \pm 0.19$	$43.81 \pm 0.50$	$45.82 \pm 0.51$

These are used to compute the six model SED curves via the [Castelli & Kurucz \(2003\)](#) stellar atmospheres. The differences between the model and measured SEDs are recorded as contributions to  $\chi^2$ . The masses, inclinations, and eccentricities are used to compute the 12  $K$  values. In turn, these are compared to the measured  $K$  values and also contribute to  $\chi^2$ . The relative weighting between the contribution to  $\chi^2$  from matching the  $K$  values vs. matching the SEDs was somewhat arbitrarily set at 80%. However, the results are insensitive to whether this relative weighting lies anywhere between 50% to 100%. We ran many MCMC chains, with between 20 and 500 million links each. To verify that the adopted relative weighting between the RV and SED contributions does not affect our conclusions, we performed additional tests in which the contribution of the RV semi-amplitudes to the total  $\chi^2$  was varied over a wide range, from 17% to 125% of the SED contribution. Over this entire range, the inferred cluster age remains remarkably stable, with an rms scatter of only  $\sim 1\%$ , and shows no systematic trend with the adopted weighting. While the absolute  $\chi^2$  values naturally change as the RV contribution is up-weighted, reflecting known tensions for two systems, the derived cluster age and stellar parameters are essentially unchanged.

The individual SEDs and their best-fitting models are shown in

Fig. 3. We find the overall quality of the fits quite satisfying. The stellar and cluster parameters derived from these fits are summarized in Table 5.

In order to quantify the sensitivity of the joint SED solution to the adopted chemical composition, we repeated the full six-binary fit across a grid of metallicities spanning  $-0.3 \leq [\text{Fe}/\text{H}] \leq +0.5$ . For each metallicity point, the cluster age was independently re-derived from its posterior age distribution. The results are shown in Fig. 4. In particular, this grid explicitly includes the solar-metallicity case, which is found to follow the same overall age–metallicity trend. Following the methodology applied in our earlier cluster studies ([Yakut et al. 2025a,b](#), see), the resulting age–metallicity relation can be described by a linear regression of the form

$$\text{Age(Gyr)} = 1.26 - 0.31 ([\text{Fe}/\text{H}] - 0.20), \quad (1)$$

or equivalently,

$$\text{Age(Gyr)} = 1.31 - 0.31 [\text{Fe}/\text{H}]. \quad (2)$$

These expressions, plotted in Fig. 4, show a mild but systematic decrease in the inferred age with increasing metallicity for  $[\text{Fe}/\text{H}] > 0$ . The minimum of the global  $\chi^2$  curve occurs near  $[\text{Fe}/\text{H}] \simeq +0.20$ ,

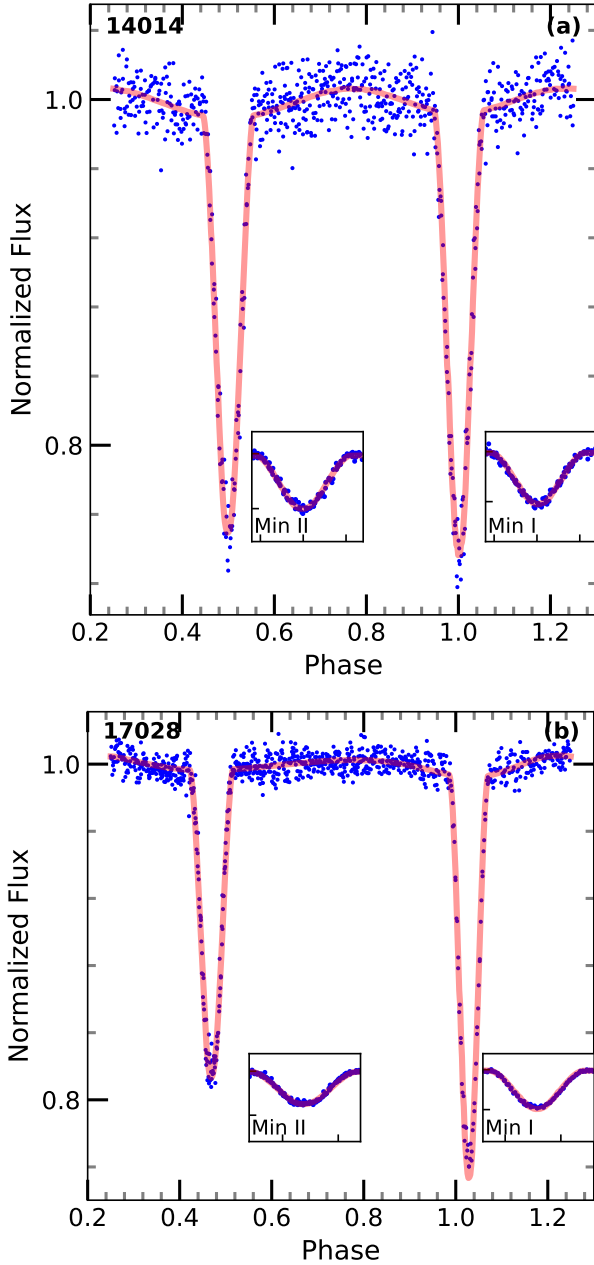


**Figure 2.** The observed and the modelled (solid lines) light curves of WOCS 14014 and WOCS 17028; insets provide zoomed views of the primary (Min I) and secondary (Min II) minima to illustrate the goodness of fit.

which we adopt as the preferred chemical composition of NGC 7789. At this metallicity, the joint SED analysis yields a cluster age of  $1.26 \pm 0.09$  Gyr (see also Fig. 4). The error bar cited here is statistical only. There is also another systematic component due to the uncertainty in metallicity of  $\sim \pm 0.1$  dex, which amounts to about 0.03 Gyr.

As mentioned above, the stellar parameters derived from the SED fitting for a fixed metallicity  $[\text{Fe}/\text{H}] = +0.2$  — masses, radii, effective temperatures, luminosities, and orbital inclinations for all twelve stars — together with the cluster-level parameters are listed in Table 5. The good agreement between the SED-based temperatures and radii and those inferred from the RV+LC analysis (for two of the binaries), as well as with the positions of the stars in the evolutionary diagrams (see

**Table 4.** Obtained fundamental parameters for WOCS 14014 and WOCS 17028 based on simultaneous LC and RV solutions. The standard errors  $1\sigma$  in the last digit are given in parentheses.

Parameter	14014	17028
Initial epoch, $T_0$ (day)	58960.8043(97)	58961.3848(74)
Period, $P$ (day)	2.3660116(4)	3.5540157(5)
Geometric parameters:		
Inclination, $i$ ( $^\circ$ )	83.1(2)	82.3(2)
Eccentricity, $e$	0.011(3)	0.110(10)
$\Omega_1$	5.535(29)	6.385(22)
$\Omega_2$	7.456(46)	7.079(29)
Fractional radii of pri.		
$R_1/a$	0.2185(13)	0.1803(7)
Fractional radii of sec.		
$R_2/a$	0.1390(11)	0.1245(6)
Radiative parameters:		
$T_{\text{eff}, 1}$ (K)	6917(123)	6727(161)
$T_{\text{eff}, 2}$ (K)	6824(121)	6442(156)
Light ratios		
$(\frac{L_1}{L_1+L_2})_{\text{TESS}}(\%)$	73	71
Mass, $M_1$ ( $M_\odot$ )	1.686(34)	1.963(23)
Radius, $R_1$ ( $R_\odot$ )	2.398(43)	2.651(55)
Luminosity, $L_1$ ( $L_\odot$ )	11.8(1.2)	12.9(1.7)
Surface gravity, $\log g_1$ (cgs)	3.906	3.885
Mass, $M_2$ ( $M_\odot$ )	1.487(30)	1.414(17)
Radius, $R_2$ ( $R_\odot$ )	1.526(27)	1.830(38)
Luminosity, $L_2$ ( $L_\odot$ )	4.5(5)	5.2(0.7)
Surface gravity, $\log g_2$ (cgs)	4.244	4.064

Sec. 6), demonstrates that the joint SED approach provides a powerful and largely independent check on the fundamental parameters of NGC 7789.

## 5 ASTROMETRIC ANALYSIS

The astrometric properties of NGC 7789 were examined using *Gaia* DR3 data in order to establish a consistent and contamination-free membership list prior to the combined RV, LC, and SED modelling. Following the procedure adopted in our earlier binary-based age studies (Yakut et al. 2025a,b), we first applied quality filters on the *Gaia* measurements—parallax uncertainties, RUWE values, and photometric excess factors—to ensure a reliable astrometric sample. Candidate members were then identified using a multidimensional selection in proper-motion space, parallax, and position on the *Gaia* CMD. This resulted in a high-probability member list of 1296 stars. The cluster’s proper-motion centroid was determined to be  $(\mu_{\alpha*}, \mu_\delta) = (-0.972 \pm 0.177, -1.894 \pm 0.166)$  mas yr $^{-1}$ , with a mean parallax of  $\varpi = 0.464 \pm 0.004$  mas, corresponding to a distance of  $2.08 \pm 0.14$  kpc, where the quoted uncertainty reflects the dispersion among member distances (standard deviation) rather than just the formal error on the mean. After defining a high-probability membership list based on *Gaia* DR3 astrometry, we adopted the individual geometric distances ( $r_{\text{geo}}$ ) from the Bailer-Jones catalogue (Bailer-Jones et al. 2021) for each confirmed member star. These geometric distances are derived from a Bayesian framework that explicitly accounts for the *Gaia* DR3 parallax zero-point offset and other known astrometric systematics, and therefore no additional parallax zero-point correction was applied in this work. These star-by-star distances incorporate *Gaia* parallax zero-point corrections and other

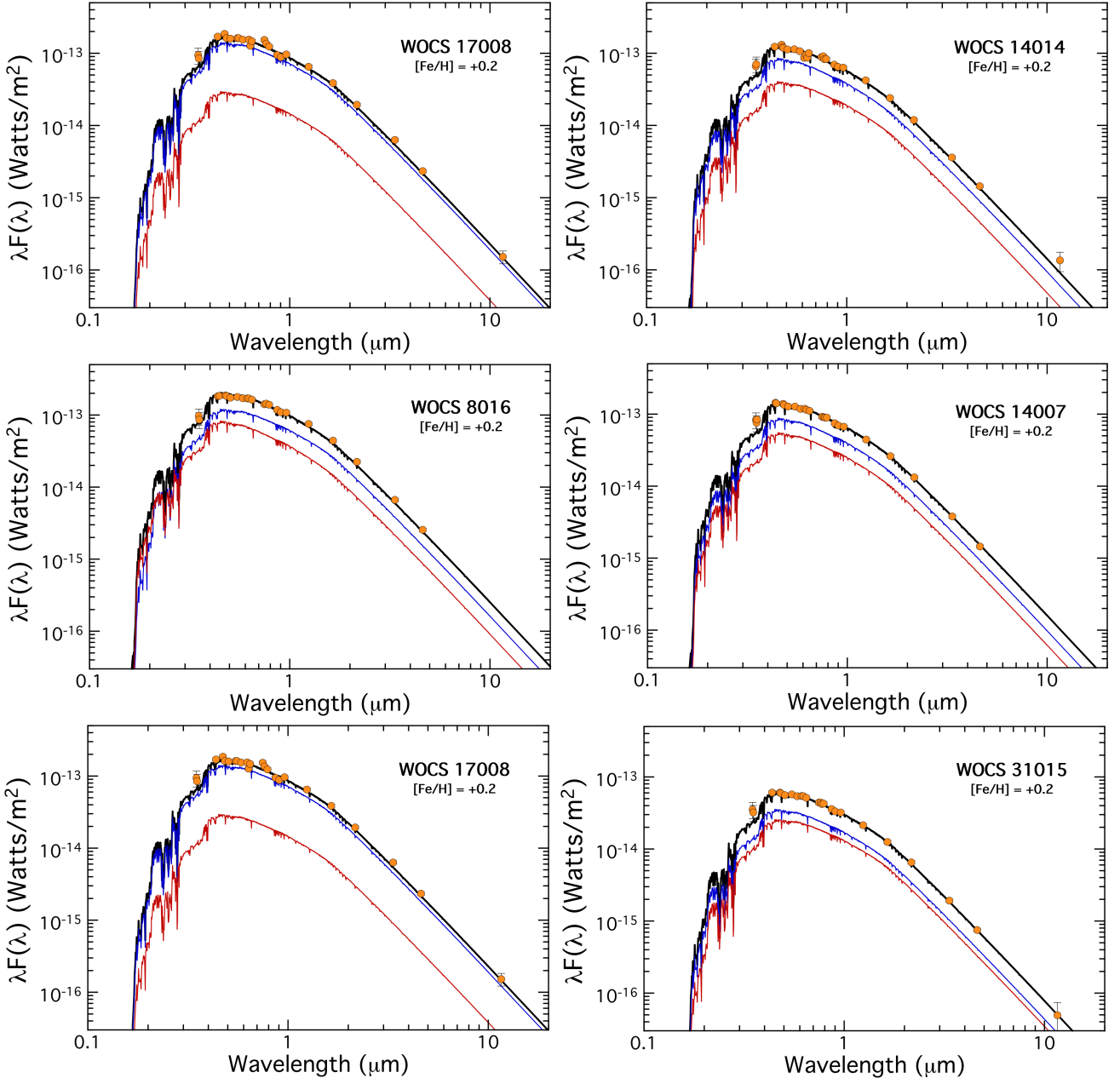


**Figure 3.** We performed a joint SED fit for six binary systems, assuming a common age, distance, and extinction ( $A_V$ ). The models were computed for a metallicity of  $[Fe/H] = 0.20$ . Figure 4 illustrates how the derived age depends on metallicity. In the figure, blue and red lines represent the best-fit models for the individual components of each binary, while the black line corresponds to the combined (composite) SED. Observational data are shown as orange circles with associated error bars.

known systematics within a Bayesian framework. The cluster distance and its uncertainty were then derived from the statistical distribution of the  $r_{\text{geo}}$  values of the selected members, rather than from a direct inversion of the mean parallax. The principal astrometric and global properties adopted for NGC 7789 are summarised in Table 6. The resulting distribution of high-probability members in proper-motion space is presented in Figure 5.

To refine the membership list further, we employed a Gaussian-mixture-based probabilistic model, assigning membership likelihoods to all stars within a radius of 20' around the cluster centre. Only stars with membership probabilities exceeding 90% were retained. This ensures that the binaries used in the subsequent SED

and RV+LC analysis are genuine cluster members sharing a common kinematic origin. The astrometric selection also helps suppress field contamination along this crowded Galactic-plane sightline, where proper-motion overlaps between field and cluster stars are substantial. The final membership list implies an expected field contamination of only about 20 stars out of 1296.

The main-sequence turnoff (MSTO), located near  $G \approx 13.8$  mag and  $(BP - RP) \approx 1.05$  mag, is fully consistent with the binary-based cluster age of  $1.26 \pm 0.09$  Gyr derived in this work, and lies within the range inferred by previous isochrone-based studies of NGC 7789. Notably, most of binaries included in our analysis are located in the evolved portion of the CMD, making them especially valuable as

**Table 5.** Derived stellar parameters for the twelve stars in our six NGC 7789 binaries from the joint SED fit. System-level components are labelled with uppercase IDs (primary = a, secondary = b). Cluster parameters from the global solution appear at the bottom. Results correspond to the adopted metallicity  $[Fe/H] = 0.20$ .

WOCS	ID	Mass ( $M_{\odot}$ )	Radius ( $R_{\odot}$ )	Temperature (K)	Luminosity ( $L_{\odot}$ )	Inclination ( $^{\circ}$ )	
17028	Aa	$1.888 \pm 0.030$	$2.962 \pm 0.143$	$6727 \pm 153$	$16.22 \pm 1.08$	$81.8 \pm 0.8$	
	Ab	$1.388 \pm 0.034$	$1.478 \pm 0.055$	$6553 \pm 75$	$3.67 \pm 0.43$	$81.8 \pm 0.8$	
14014	Ba	$1.779 \pm 0.032$	$2.423 \pm 0.110$	$6917 \pm 123$	$12.16 \pm 0.96$	$82.2 \pm 0.8$	
	Bb	$1.532 \pm 0.033$	$1.745 \pm 0.064$	$6802 \pm 64$	$5.92 \pm 0.58$	$82.2 \pm 0.8$	
8016	Ca	$1.928 \pm 0.039$	$3.252 \pm 0.169$	$6600 \pm 130$	$18.15 \pm 1.56$	$73.9 \pm 2.8$	
	Cb	$1.767 \pm 0.038$	$2.382 \pm 0.150$	$6919 \pm 126$	$11.77 \pm 1.19$	$73.9 \pm 2.8$	
14007	Da	$1.790 \pm 0.043$	$2.474 \pm 0.159$	$6900 \pm 130$	$12.56 \pm 1.38$	$44.3 \pm 1.5$	
	$1.628 \pm 0.057$	$1.968 \pm 0.139$	$6892 \pm 85$	$7.97 \pm 1.30$	$44.3 \pm 1.5$		
17008	Ea	$1.962 \pm 0.041$	$3.531 \pm 0.186$	$6591 \pm 155$	$21.23 \pm 1.54$	$54.5 \pm 1.2$	
	Eb	$1.441 \pm 0.044$	$1.570 \pm 0.069$	$6660 \pm 91$	$4.43 \pm 0.60$	$54.5 \pm 1.2$	
31015	Fa	$1.494 \pm 0.028$	$1.669 \pm 0.049$	$6749 \pm 59$	$5.25 \pm 0.44$	$64.1 \pm 1.7$	
	Fb	$1.405 \pm 0.028$	$1.507 \pm 0.045$	$6589 \pm 63$	$3.89 \pm 0.37$	$64.1 \pm 1.7$	
		Age (Myr)		$A_V$ (mag)			
		$1257 \pm 90$		$0.90 \pm 0.05$			

Notes: The distance prior was tightly constrained around the Gaia distance of  $2080 \pm 142$  pc, and the metallicity was fixed at  $[Fe/H] = +0.2$  (but see Figure 4 for an exploration of the cluster metallicity.)

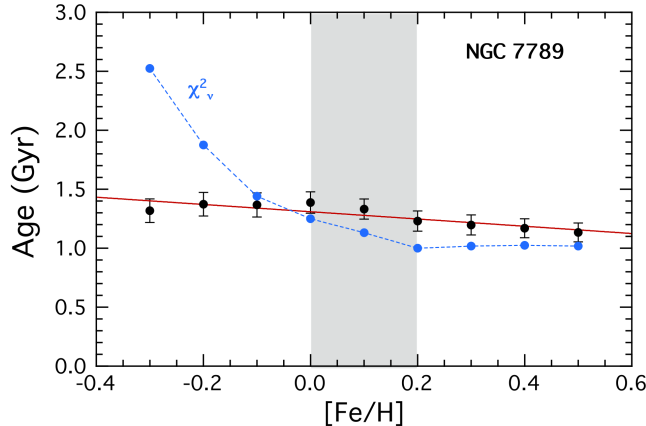


**Figure 4.** Age of NGC 7789 vs. the assumed metallicity  $[Fe/H]$ . The same type of SED fits used to produce Table 5 and Fig. 3 was carried out for additional metallicities. We find a linear relation between the age of NGC 7789 and metallicity given in Sec. 4. The  $\chi^2$  value at each metallicity tested is also plotted to provide an idea of which metallicities are acceptable, i.e., for  $[Fe/H] \gtrsim 0$ .

**Table 6.** Summary of the astrometric, kinematic, and global properties adopted for NGC 7789.

Parameter	Value
Cluster centre RA (J2000)	$23^{\text{h}}57^{\text{m}}24^{\text{s}}$
Cluster centre Dec (J2000)	$+56^{\circ}42'30''$
$\mu_{\alpha^*}$ (mas yr $^{-1}$ )	$-0.972 \pm 0.177$
$\mu_{\delta}$ (mas yr $^{-1}$ )	$-1.894 \pm 0.166$
Mean parallax $\varpi$ (mas)	$0.464 \pm 0.004$
Distance (kpc)	$2.08 \pm 0.14$
Mean radial velocity $\langle V_r \rangle$ (km s $^{-1}$ )	$-54.9 \pm 0.5$
Binary-based age (Gyr)	$1.26 \pm 0.09$
Number of Gaia DR3 members	1296

independent age diagnostics, since their radii and masses can be determined dynamically.

Finally, the astrometric analysis provides the global cluster framework adopted as external priors in our combined SED and RV+LC modelling. The cluster distance of  $2.08 \pm 0.14$  kpc, derived from Gaia DR3 astrometry, was used as a tight prior in the SED analysis, thereby defining the common geometric scale for all six binary systems. The line-of-sight extinction was allowed to vary within a broad prior range ( $A_V = 0.74\text{--}0.98$  mag), and the joint SED fitting converged on  $A_V = 0.90 \pm 0.05$  mag, fully consistent with the adopted prior and with the cluster colour-magnitude diagram morphology. The agreement between the astrometric framework and the binary-based modelling demonstrates that the inferred stellar and cluster parameters are mutually consistent within a single, coherent solution for NGC 7789.

## 6 RESULTS AND CONCLUSION

We have carried out a comprehensive determination of the fundamental parameters of the open cluster NGC 7789 by jointly analysing six well-characterised binary systems using radial velocity (RV) measurements, TESS photometry, and broadband spectral energy distributions. This work extends the binary-based SED+LC+RV methodology introduced by our team in recent cluster studies, where it successfully yielded high-precision, model-independent ages for both the old benchmark cluster NGC 188 (Yakut et al. 2025a) and the intermediate-age system NGC 2506 (Yakut et al. 2025b). Applied to NGC 7789, this framework provides an alternative and complementary route to conventional isochrone-only techniques by leveraging the absolute masses, radii, and luminosities of evolved detached binaries.

With the SEDs for all six targets, and incorporating the latest dynamical constraints, our joint modelling converges on a cluster age of  $1.26 \pm 0.09$  Gyr. This value lies at the younger end of, but remains consistent with, the canonical 1.2–1.6 Gyr range inferred from modern Gaia-based isochrone analyses (e.g., Dias et al. 2021; Balan et al. 2024; Ferreira et al. 2025). The age–metallicity trend obtained from

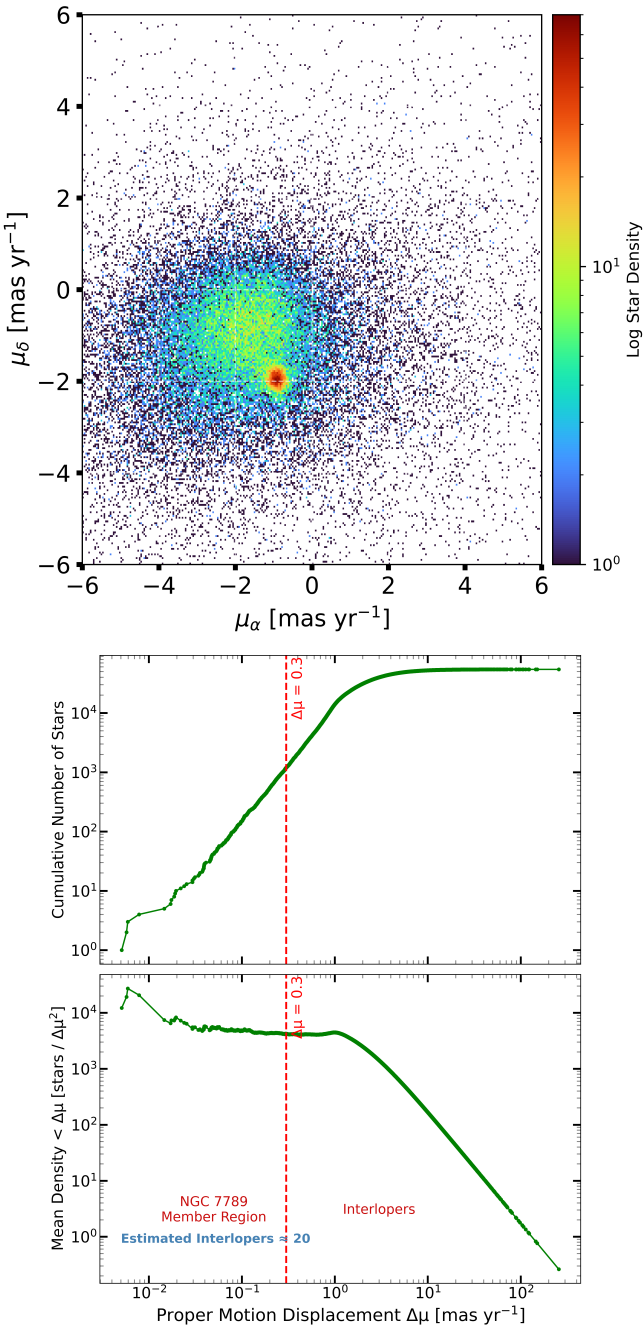


**Figure 5.** **Top:** Proper-motion density map of the NGC 7789 field based on *Gaia* DR3 data. The cluster population is clearly identified as the prominent red overdensity centred at  $(\mu_{\alpha^*}, \mu_\delta) \approx (-0.97, -1.89)$  mas yr $^{-1}$ , corresponding to the mean cluster motion. **Middle:** Cumulative distribution of proper-motion displacements  $\Delta\mu$  from the cluster centroid. The vertical dashed line at  $\Delta\mu = 0.3$  mas yr $^{-1}$  marks the adopted membership boundary separating the dense cluster core from the surrounding field population. **Bottom:** Mean cumulative density (number of stars per  $\Delta\mu^2$ ) as a function of  $\Delta\mu$ , showing a rapid decline in source density beyond the adopted cutoff and confirming the effectiveness of the membership selection.

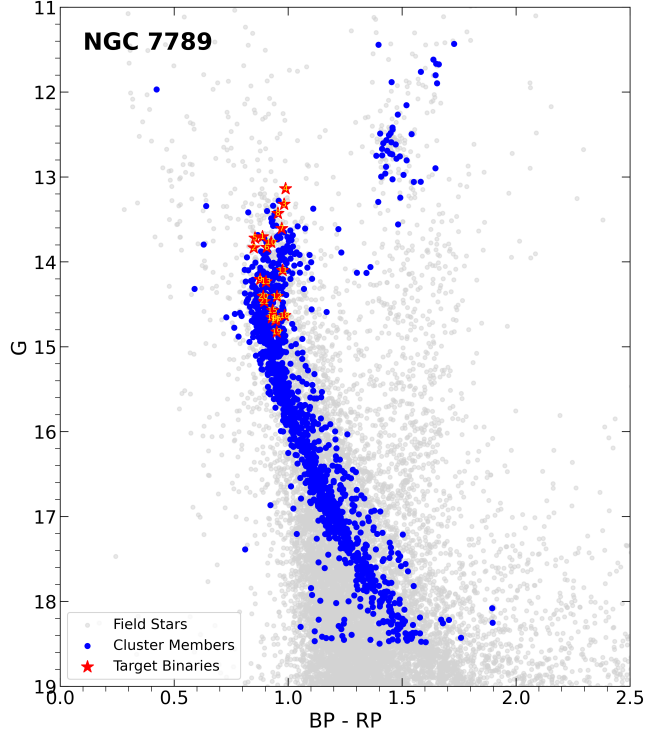


**Figure 6.** Colour-magnitude diagram of NGC 7789 based on *Gaia* DR3 photometry. The vertical axis shows the  $G$  magnitude. All sources within a 20-arcmin radius of the cluster centre are shown in gray, while high-probability members selected through astrometric and photometric criteria are highlighted in blue. The twelve stars of the six target binaries are marked as red star symbols with overplotted numeric labels corresponding to their IDs. Most of these binary components are evolved stars located close to the cluster main-sequence turnoff, where age sensitivity is maximised.

the six binaries shows a weak but systematic decline in age with increasing  $[\text{Fe}/\text{H}]$ , and the global  $\chi^2$  minimum indicates a preferred metallicity of  $[\text{Fe}/\text{H}] \approx +0.20$ . This value lies within  $2-3\sigma$  of the uncertainties of published spectroscopic measurements (Tautvaišienė et al. 2005a; Overbeek et al. 2015; Carrera & Martínez-Vázquez 2013) and produces excellent agreement between the predicted and observed radii and effective temperatures of all binary components.

The joint analysis further demonstrates that the stellar parameters inferred from the binaries are fully consistent with the astrometric properties of the cluster. The *Gaia* DR3 distance of  $2082 \pm 142$  pc, adopted as an external prior in the SED modelling, is entirely compatible with the luminosities and radii inferred for all six binary systems. Within this framework, the SED fitting converges on a line-of-sight extinction of  $A_V = 0.90 \pm 0.05$  mag, which lies comfortably within the adopted prior range and is consistent with literature reddening estimates as well as with the observed cluster sequence in the *Gaia* colour-magnitude diagram. This agreement confirms that the binary-based modelling and the astrometric constraints together define a coherent and self-consistent global solution for NGC 7789.

The SED fits yield mutually consistent stellar parameters for all six systems. Only one source, WOCS 17028, shows a residual discrepancy at the  $\sim 2\sigma$  level between the stellar masses inferred from the radial-velocity orbit and those implied by the SED-based modelling. Given its broad photometric wavelength coverage, such a mismatch is plausibly explained by a modest level of unrecognised third-light contamination rather than a deficiency in the binary evolution mod-

elling. Crucially, excluding this system from the joint analysis leaves the derived cluster parameters well within the uncertainties, demonstrating the robustness and redundancy of the multi-binary approach.

It is also worth mentioning that for four of the six systems, reliable stellar masses were obtained without relying on inclination angles derived from eclipses or ellipsoidal variability. In these cases, the combination of double-lined spectroscopic orbits with the joint SED constraints is sufficient to determine both the component masses and the inclination angles. This is possible because the RVs provide the mass ratios which are crucial to separating the contribution from the two stars in a given composite SED. This underscores the applicability of the method to non-eclipsing binaries.

Overall, NGC 7789 becomes the third open cluster for which the SED+LC+RV framework delivers high-precision and physically well-constrained stellar and cluster parameters—frequently with more reliable age constraints than those available from isochrone fitting alone. The strong internal consistency between the binary-derived age, reddening, and adopted metallicity underscores the diagnostic power of evolved detached binaries in intermediate-age clusters. Future high-resolution spectroscopy and additional long-period binary characterisation within NGC 7789 will further refine the cluster metallicity and may reduce the remaining statistical uncertainties in the age determination.

## ACKNOWLEDGEMENTS

We thank the anonymous referee for their careful reading of the manuscript and for several constructive comments that helped to improve the clarity and robustness of this work. This work has made use of data from the European Space Agency (ESA) *Gaia* mission (<https://www.cosmos.esa.int/gaia>), processed by the *Gaia* Data Processing and Analysis Consortium (DPAC); <https://www.cosmos.esa.int/web/gaia/dpac/consortium>). It also makes use of observations obtained with the Transiting Exoplanet Survey Satellite (*TESS*) mission, funded by the NASA Explorer Program and publicly available through the Mikulski Archive for Space Telescopes (MAST). This research has made use of the SIMBAD and VizieR catalogues operated at the Centre de Données astronomiques de Strasbourg (CDS), and of NASA’s Astrophysics Data System (ADS) bibliographic services. This study was supported by the Scientific and Technological Research Council of Türkiye (TÜBİTAK, grant numbers 112T766, 117F188 and 2219). Numerical computations were performed in part using the High Performance and Grid Computing Center (TRUBA resources) provided by TÜBİTAK ULAKBİM. KY gratefully acknowledges the Master and Fellows of Churchill College, University of Cambridge, for the award of an Overseas Research Fellowship.

## DATA AVAILABILITY

The *TESS* observations used in the analysis of binary light curves are available online to the public through the Mikulski Space Telescope Archive (MAST). If desired, the data used in this study can be obtained from the MAST servers or requested from the authors.

## REFERENCES

Anthony-Twarog B. J., Brunker S. W., Deliyannis C. P., Rich E., Steinhauer A., Sun Q., Twarog B. A., 2025, arXiv e-prints, p. arXiv:2510.25862

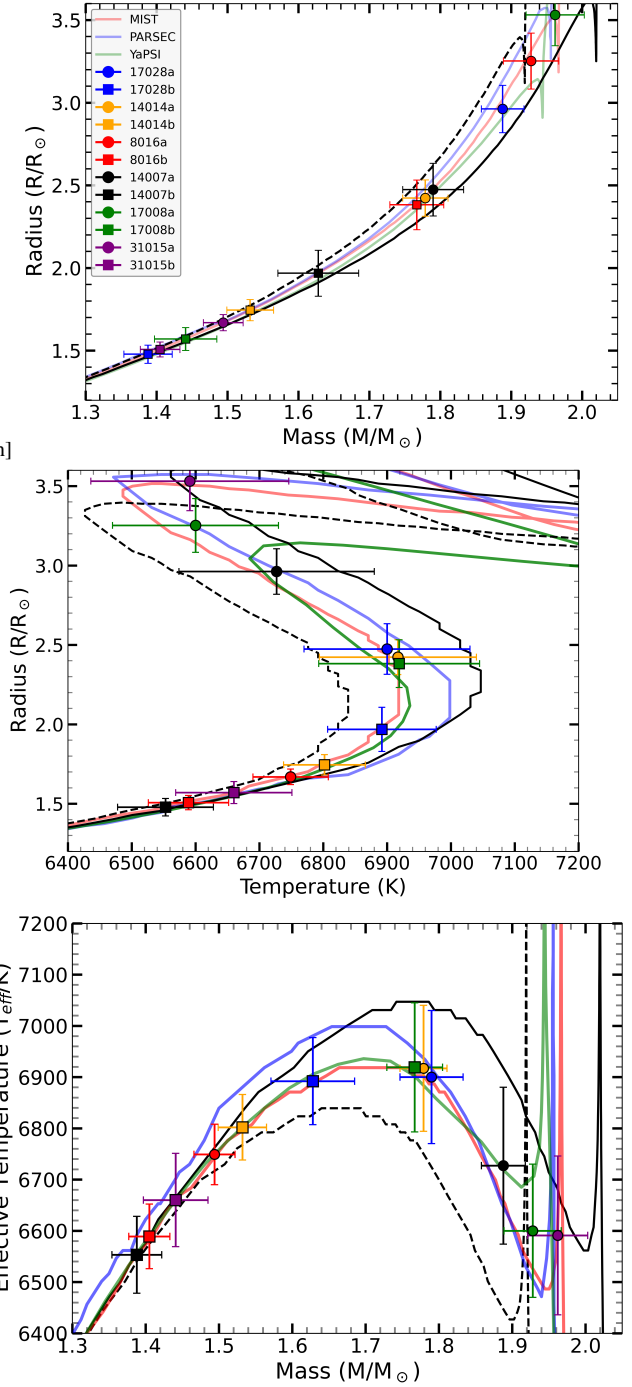


**Figure 7.** Radius–Mass, Radius–Temperature, and Temperature–Mass diagrams for the six binary systems analysed in NGC 7789. Each binary component is shown as a different color marker. Stellar evolution isochrones from MIST (red solid), PARSEC (blue dashed), and YaPSI/Y<sup>2</sup> (green dashed) for an age of  $1.26 \pm 0.09$  Gyr are overplotted. To illustrate the age uncertainty range, additional MIST isochrones at ages of 1.32 Gyr (black dashed) and 1.14 Gyr (black solid) are included. The parameters of all six binaries are listed in Table 5.

Bailer-Jones C. A. L., Rybizki J., Fouesneau M., Demleitner M., Andrae R., 2021, [AJ, 161, 147](#)

Balan S., Rao K. K., Vaidya K., Agarwal M., Bhattacharya S., 2024, [AJ, 168, 204](#)

Bianchi L., Shiao B., Thilker D., 2017, [ApJS, 230, 24](#)

Burbidge E. M., Sandage A., 1958, [ApJ, 128, 174](#)

Cantat-Gaudin T., et al., 2018, [A&A, 618, A93](#)

Cantat-Gaudin T., et al., 2020, [A&A, 640, A1](#)

Carbajo-Hijarrubia J., et al., 2024, [A&A, 687, A239](#)

Cardelli J. A., Clayton G. C., Mathis J. S., 1989, [ApJ, 345, 245](#)

Carrera R., Martínez-Vázquez C. E., 2013, [A&A, 560, A5](#)

Castelli F., Kurucz R. L., 2003, in Piskunov N., Weiss W. W., Gray D. F., eds, IAU Symposium Vol. 210, Modelling of Stellar Atmospheres. p. A20

Chambers K. C., Magnier E. A., Metcalfe N. e. a., 2016, arXiv e-prints,

Choi J., Dotter A., Conroy C. e. a., 2016, [ApJ, 823, 102](#)

Cutri R. M., Wright E. L., Conrow T. e. a., 2013, Explanatory Supplement to the AllWISE Data Release Products

Dias W. S., Monteiro H., Moitinho A., Lépine J. R. D., Carraro G., Paunzen E., Alessi B., Villegas L., 2021, [MNRAS, 504, 356](#)

Dotter A., 2016, [ApJS, 222, 8](#)

Ferraro F. R., et al., 2009, [Nature, 462, 1028](#)

Ferreira F. A., Santos J. F. C., Corradi W. J. B., Angelo M. S., Maia F. F. S., 2025, [MNRAS, 539, 265](#)

Friel E. D., Janes K. A., Tavarez M., Scott J., Katsanis R., Lotz J., Hong L., Miller N., 2002, [AJ, 124, 2693](#)

Gaia Collaboration et al., 2023, [A&A, 674, A1](#)

Gao X.-h., 2018, [PASP, 130, 124101](#)

Gim M., Hesser J. E., McClure R. D., Stetson P. B., 1998, [PASP, 110, 1172](#)

Gunn J. E., et al., 1998, [AJ, 116, 3040](#)

Henden A. A., Templeton M., Terrell D., Smith T. C., Levine S., Welch D., 2016, VizieR Online Data Catalog: AAVSO Photometric All Sky Survey (APASS) DR9 (Henden+, 2016), VizieR On-line Data Catalog: II/336. Originally published in: 2015AAS...22533616H

Hurley J. R., Tout C. A., Aarseth S. J., Pols O. R., 2001, [MNRAS, 323, 630](#)

Jacobson H. R., Pilachowski C. A., Friel E. D., 2011, [AJ, 142, 59](#)

Martinez Roger C., Paez E., Castellani V., Straniero O., 1994, [A&A, 290, 62](#)

Mazzei P., Pigatto L., 1988, [A&A, 193, 148](#)

Nagarajan N., Sneden C., Afşar M., Pilachowski C. A., 2023, [AJ, 165, 245](#)

Nine A. C., Milliman K. E., Mathieu R. D., Geller A. M., Leiner E. M., Platais I., Tofflemire B. M., 2020, [AJ, 160, 169](#)

Nine A. C., Mathieu R. D., Schuler S. C., Milliman K. E., 2024, [ApJ, 970, 187](#)

Ochsenbein F., Bauer P., Marcout J., 2000, [A&AS, 143, 23](#)

Overbeek J. C., Friel E. D., Jacobson H. R., Johnson C. I., Pilachowski C. A., Mészáros S., 2015, [AJ, 149, 15](#)

Pancino E., Carrera R., Rossetti E., Gallart C., 2010, [A&A, 511, A56](#)

Paxton B., Bildsten L., Dotter A., Herwig F., Lesaffre P., Timmes F., 2011, [ApJS, 192, 3](#)

Paxton B., et al., 2015, [ApJS, 220, 15](#)

Paxton B., et al., 2019, [ApJS, 243, 10](#)

Perets H. B., Fabrycky D. C., 2009, [ApJ, 697, 1048](#)

Skrutskie M. F., et al., 2006, [AJ, 131, 1163](#)

Spina L., et al., 2021, [MNRAS, 503, 3279](#)

Tautvaišienė G., Edvardsson B., Puzeras E., Ilyin I., 2005a, [A&A, 431, 933](#)

Tautvaišienė G., Edvardsson B., Puzeras E., Ilyin I., 2005b, [A&A, 431, 933](#)

Vaidya K., Panthi A., Agarwal M., Pandey S., Rao K. K., Jadhav V., Subramaniam A., 2022, [MNRAS, 511, 2274](#)

Vaidya K., Panthi A., Jadhav V., Kunwar Rao K., Pandey S., Subramaniam A., Agarwal M., 2024, [Bulletin de la Societe Royale des Sciences de Liege, 93, 250](#)

Yakut K., et al., 2009, [A&A, 503, 165](#)

Yakut K., Eggleton P. P., Kalomeni B., Tout C. A., Eldridge J. J., 2015, [MNRAS, 453, 2937](#)

Yakut K., Kalomeni B., Rappaport S., 2025a, [MNRAS, 542, 1817](#)

Yakut K., Kalomeni B., Rappaport S., Kostov V., 2025b, [MNRAS, 544, 271](#)

de Juan Ovelar M., et al., 2020, [MNRAS, 491, 2129](#)

This paper has been typeset from a  $\text{\TeX}/\text{\LaTeX}$  file prepared by the author.